Plasma Phys. Control. Fusion **49** (2007) 1177–1191 doi:10.1088/0741-3335/49/8/006

Fluid magnetohydrodynamic stability in a Heliotron with anisotropic fast particle species

W A Cooper[1], J P Graves[1], M Jucker[1], K Y Watanabe[2], Y Narushima[2] and T Yamaguchi[3]

[1] Ecole Polytechnique Fédérale de Lausanne, Centre de Recherches en Physique des Plasmas, Association Euratom-Suisse, CH1015 Lausanne, Switzerland
[2] National Institute for Fusion Science, Oroshi-cho 322-6, Toki 509-5292, Japan
[3] The Graduate School for Advanced Studies, Oroshi-cho 322-6, Toki 509-5292, Japan

E-mail: wilfred.cooper@epfl.ch

Received 16 April 2007, in final form 7 June 2007
Published 3 July 2007
Online at stacks.iop.org/PPCF/49/1177

Abstract

The local and global fluid magnetohydrodynamic stability properties of anisotropic pressure plasmas are investigated with the Kruskal–Oberman and rigid hot particle Johnson *et al* energy principles. A Heliotron configuration that models the Large Helical Device with finite pressure anisotropy driven by neutral beams at $\langle\beta\rangle = 4\%$ shows that the Kruskal–Oberman model predicts stability when $\langle\beta^{\mathrm{h}}\rangle/\langle\beta\rangle \sim 1/3$ provided that the hot particle pressure profile is sufficiently peaked. The rigid hot particle model, on the other hand, is stable to local and global modes for broad and peaked profiles. For central deposition, the marginal pressure profiles are somewhat broader for $p_\parallel > p_\perp$ than for $p_\perp > p_\parallel$. Global $n = 3$ modes produce stricter stability criteria than $n = 1, 2$ and 4 modes. Off-axis hot particle deposition yields more unstable conditions with respect to global and local modes than on-axis deposition. The mode structures localize near the plasma periphery according to the Kruskal–Oberman model and near the plasma core according to the Johnson *et al* model. This observation could help resolve the appropriate model to apply to the experimental conditions in Heliotron devices.

1. Introduction

Negative ion tangential neutral beam injection with 10 MW and 180 keV have produced Large Helical Device (LHD) plasmas with $\langle\beta\rangle \geqslant 4\%$ [1]. The electron density in the discharges of $1 \times 10^{19}\ \mathrm{m}^{-3} \leqslant \langle N_{\mathrm{e}}\rangle \leqslant 3 \times 10^{19}\ \mathrm{m}^{-3}$ has shown significant levels of anisotropy with $T_\parallel > T_\perp$, where $T_\parallel (T_\perp)$ corresponds to the parallel (perpendicular) temperature [2]. Furthermore, the fast particles contribute about a $1/3$ fraction of the total $\langle\beta\rangle$. There are also clear indications not only that the ideal magnetohydrodynamic (MHD) stability model predictions for both local and global mode structures have been violated in high-$\langle\beta\rangle$ experimental discharges but also

that a model which would treat the energetic particle species as a rigid non-interacting fluid fits the experimental data quite accurately [1].

Two fluid stability models that extend beyond ideal MHD have been considered to treat three-dimensional (3D) plasmas with pressure anisotropy. The Kruskal–Oberman energy principle (in which we ignore a non-fluid Kinetic energy integral term related to trapped particle effects) models the hot particle population as a fully interacting fluid element [3,4]. The Johnson–Kulsrud–Weimer energy principle treats the energetic particle pressures and currents as a rigid non-interacting layer [5, 6]. The energetic particle species are described with a modified bi-Maxwellian distribution function [7–9] which satisfies the solution of the Fokker–Planck equation to lowest order. Analytic expressions for the parallel and perpendicular pressure moments can be obtained with this distribution function which allows a description of the equilibrium properties and the implementation in the 3D VMEC code that assumes nested flux surfaces [10]. The determination whether either one of these models is able to reproduce the experimental conditions observed in the LHD constitutes a motivating factor for the research activity undertaken in this paper.

The principal aim for the application of neutral beams and radio frequency waves in magnetic confinement systems constitutes the heating of plasmas to thermonuclear temperatures. For this purpose, the generation of energetic particles in the core region of the plasma is desirable. However, issues related to rotational transform profile control make off-axis fast particle deposition a relevant option to investigate in detail.

We concentrate on the examination of cases with large parallel and perpendicular pressure anisotropies in a 10-field period Heliotron that serves as a model for LHD [11] at $\langle\beta\rangle \simeq 4\%$ and $\langle\beta_{\rm th}\rangle \simeq 2.6\%$. A comparison of high field (HF) and low field (LF) energetic particle deposition with respect to the equilibrium and fluid stability properties using the Kruskal–Oberman and Johnson *et al* models is undertaken. The results are also compared with a reference on-axis hot particle calculation. Hot particle pressure profile effects on the fluid MHD stability for large parallel and perpendicular anisotropies are also analysed for central fast particle deposition.

2. Pressure moments of the bi-maxwellian distribution function

A variant of the bi-Maxwellian distribution function given by

$$\mathcal{F}_{\rm h}(s,\mathcal{E},\mu) = \mathcal{N}(s)\left(\frac{m_h}{2\pi T_\perp(s)}\right)^{3/2} \exp\left[-m_{\rm h}\left(\frac{\mu B_{\rm C}}{T_\perp(s)} + \frac{|\mathcal{E}-\mu B_{\rm C}|}{T_\parallel(s)}\right)\right] \tag{1}$$

is applied to model the hot particle species and satisfies the lowest order solution of the Fokker–Planck equation [7]. A bi-Maxwellian distribution function of this form very adeptly models the effects of ion cyclotron resonance heating [7–9]. However, it may also adequately though perhaps not quite so accurately represent the impact of neutral beam heating. The parallel pressure moment corresponds to

$$p_\parallel(s,B) = p(s) + \mathcal{N}(s)T_\parallel(s)H(s,B), \tag{2}$$

where $p(s)$ is the pressure from the thermal species of the plasma, s is the radial variable proportional to the enclosed toroidal magnetic flux $2\pi\Phi$ and the hot particle functional $H(s,B)$, which makes the pressures vary around a flux surface, is written for $B > B_{\rm C}$ as

$$H(s,B) = \frac{(B/B_{\rm C})}{\left[1 - \dfrac{T_\perp}{T_\parallel}\left(1 - \dfrac{B}{B_{\rm C}}\right)\right]}, \tag{3}$$

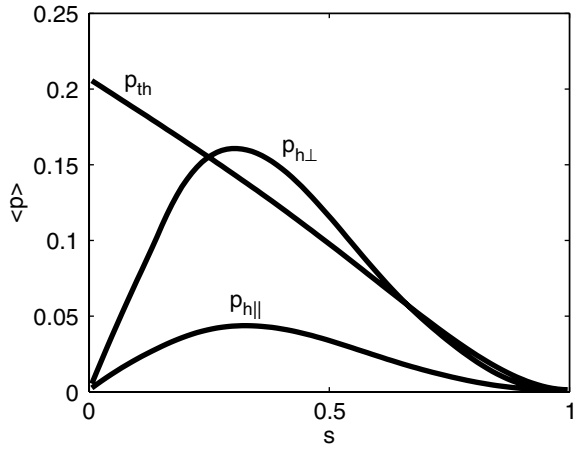

Figure 1. Typical flux surface averaged pressure profiles with HF side hot particle deposition and $p_\perp > p_\parallel$. The perpendicular (parallel) hot particle pressure is labelled as $p_{\mathrm{h}\perp}(p_{\mathrm{h}\parallel})$ while the thermal pressure is $p_{\mathrm{th}} \equiv p(s)$.

while for $B < B_{\mathrm{C}}$ as

$$H(s, B) = \frac{B}{B_{\mathrm{C}}} \frac{\left[1 + \dfrac{T_\perp}{T_\parallel}\left(1 - \dfrac{B}{B_{\mathrm{C}}}\right) - 2\left(\dfrac{T_\perp}{T_\parallel}\right)^{5/2}\left(1 - \dfrac{B}{B_{\mathrm{C}}}\right)^{5/2}\right]}{\left[1 - \left(\dfrac{T_\perp}{T_\parallel}\right)\left(1 - \dfrac{B}{B_{\mathrm{C}}}\right)\right]\left[1 + \left(\dfrac{T_\perp}{T_\parallel}\right)\left(1 - \dfrac{B}{B_{\mathrm{C}}}\right)\right]}. \tag{4}$$

The critical magnetic field B_{C} identifies and controls the hot particle deposition layer. The perpendicular pressure moment is calculated from parallel force balance.

3. The equilibrium state

The 3D VMEC equilibrium code [12] has been adapted to investigate the equilibrium properties of stellarator systems with energetic particle species whose pressures can be described by the appropriate moments of the bi-Maxwellian distribution function presented in the previous section [10]. The MHD equilibria are produced by minimizing the energy functional

$$W = \int\int\int \mathrm{d}^3x \left(\frac{B^2}{2\mu_0} + \frac{p_\parallel(s, B)}{\Gamma - 1}\right), \tag{5}$$

where $\mu_0 = 4\pi \times 10^{-7}\,\mathrm{H\,m^{-1}}$ is the permeability of free space. We typically take the adiabatic index $\Gamma = 0$; therefore, the total parallel pressure can be written as $p_\parallel(s, B) = p(s)[1 + p_{\mathrm{h}}(s)H(s, B)]$. It is useful to note that this expression can be reconciled with that obtained from the parallel pressure moment of the bi-Maxwellian distribution function with the identification $\mathcal{N}(s)T_\parallel(s) = p(s)p_{\mathrm{h}}(s)$, where $p_{\mathrm{h}}(s)$ is a factor that scales the hot particle pressures. The ratio of the hot particle perpendicular to parallel temperature $T_\perp/T_\parallel$, the effective toroidal current density $2\pi J$ and the critical field B_{C} constitute together with p and p_{h} the input profiles to describe the equilibrium state. For simplicity, we have chosen B_{C} and $T_\perp/T_\parallel$ as constant parameters in the calculations undertaken in this study. A typical set of flux surface averaged profiles for the thermal, hot perpendicular and parallel pressures are displayed in figure 1 for a case with off-axis hot particle deposition and $p_\perp > p_\parallel$.

4. Fluid MHD stability

The Kruskal–Oberman (KO) and Johnson–Kulsrud–Weimer (NI) models to treat anisotropic pressure plasma stability have been implemented in the TERPSICHORE code [13] for the computation of fluid MHD stability properties of 3D plasma confinement configurations. The variational form can be represented as the eigenvalue problem

$$\langle \delta W_{\mathrm{P}} \rangle + \langle \delta W_{\mathrm{V}} \rangle - \omega^2 \langle \delta W_{\mathrm{K}} \rangle = 0, \tag{6}$$

$$\langle \delta W_{\mathrm{P}} \rangle = \langle \delta W_{\mathrm{C}^2} \rangle + \langle \delta W_{\mathrm{BI}} \rangle + \langle \delta W_{\mathrm{J}} \rangle, \tag{7}$$

where δW_{P} constitutes the internal plasma potential energy, δW_{V} is the vacuum energy and $-\omega^2 \delta W_{\mathrm{K}}$ is the kinetic energy. As in the ideal MHD model [14], the internal plasma potential energy can be broken into a positive definite term (δW_{C^2}) which involves stabilizing contributions from the twisting, bending and compression of the magnetic field lines, (δW_{BI}) which is associated with the interaction of the pressure gradients with the magnetic field line curvature and the parallel current kink instability term (δW_{J}). Local fluid stability properties can be evaluated with the Mercier criterion. The equations that describe the Mercier criterion according to the KO and NI models that we investigate have been derived and presented in [13].

4.1. The ballooning-interchange instability drive

The driving term for ballooning and interchange modes according to the KO model is expressed in Boozer magnetic coordinates [15] on each flux surface as

$$\begin{aligned}\delta W_{\mathrm{BI}}(s) = -\frac{1}{2}\int_0^{\frac{2\pi}{L_s}} \mathrm{d}\phi \int_0^{2\pi} \mathrm{d}\theta \left(\frac{\tau}{\tau+\sigma}\right)\left(\frac{1}{\sigma B^2}\right)\left(\frac{\partial p_\parallel}{\partial s}\bigg|_B + \frac{\sigma}{\tau}\frac{\partial p_\perp}{\partial s}\bigg|_B\right)(\xi^s)^2 \\ \times\left[\sqrt{g}\left(\frac{\partial p_\parallel}{\partial s}\bigg|_B + \frac{\sigma}{\tau}\frac{\partial p_\perp}{\partial s}\bigg|_B\right) + \psi''(s)J(s) - \Phi''(s)I(s) + \psi'(s)J'(s) - \Phi'(s)I'(s)\right. \\ \left. + \sigma B_s(\boldsymbol{B}\cdot\boldsymbol{\nabla}\sqrt{g}) - \sigma B^2\frac{\partial\sqrt{g}}{\partial s}\right],\end{aligned} \tag{8}$$

while the corresponding counterpart for the NI model is

$$\begin{aligned}\delta W_{\mathrm{BI}}(s) = -\frac{1}{2}\int_0^{\frac{2\pi}{L_s}} \mathrm{d}\phi \int_0^{2\pi} \mathrm{d}\theta \frac{p'(s)}{\sigma B^2}\left[\sqrt{g}\left(\frac{\partial p_\parallel}{\partial s}\bigg|_B + \sigma p'(s)\right) + \psi''(s)J(s) - \Phi''(s)I(s)\right. \\ \left. + \psi'(s)I'(s) - \Phi'(s)J'(s) + \sigma B_s(\boldsymbol{B}\cdot\boldsymbol{\nabla}\sqrt{g}) - \sigma B^2\frac{\partial\sqrt{g}}{\partial s}\right](\xi^s)^2,\end{aligned} \tag{9}$$

where θ and ϕ are the Boozer poloidal and toroidal angles, respectively, $2\pi\psi$, $2\pi I$ and $2\pi J$ are the poloidal magnetic flux, the effective poloidal current flux and the effective toroidal current flux, respectively, $\sqrt{g}$ is the Jacobian of the transformation from a Cartesian grid to the Boozer coordinate frame and ξ^s is the radial displacement vector in contravariant representation. The symbol prime ($'$) denotes the derivative of a flux surface quantity with respect to s and L_s is the number of equilibrium field periods that fit within one period of the instability structure. The functions σ and τ correspond to the firehose and mirror stability criterion parameters [10, 16]. They correspond to $1/\mu_0$ when $p_\parallel = p_\perp$. B_s is the radial component of the magnetic field in the covariant representation.

In the KO model, the combined pressure $p_\parallel$ and $p_\perp$ gradients of the thermal species and hot particles drive ballooning and interchange modes through their contribution to δW_{BI}. In the NI

model, the thermal pressure p gradients contribute dominantly to $\delta W_{\rm BI}$. In fact, an integration by parts and equilibrium radial force balance can explicitly eliminate the radial gradient of the total parallel pressure in equation (9). In that sense, the hot particle pressure gradients appear only indirectly through their effect on the equilibrium properties of the system in this model.

4.2. The parallel current density kink instability drive

The driving term for parallel current density kink instabilities that can be extracted in the Boozer coordinate frame within the KO energy principle is

$$\delta W_{\rm J}(s) = -\frac{1}{2}\int_0^{\frac{2\pi}{L_s}} {\rm d}\phi \int_0^{2\pi} {\rm d}\theta \frac{\boldsymbol{K}\cdot\boldsymbol{B}}{B^2}\left[\frac{\sqrt{g}B^2}{\sigma|\boldsymbol{\nabla}s|^2}\left(\frac{\boldsymbol{K}\cdot\boldsymbol{B}}{B^2}\right) + \psi'(s)\Phi''(s) - \Phi'(s)\psi''(s)\right](\xi^s)^2$$
$$-\frac{1}{2}\int_0^{\frac{2\pi}{L_s}} {\rm d}\phi \int_0^{2\pi} {\rm d}\theta \frac{\boldsymbol{K}\cdot\boldsymbol{B}}{B^2} h_s\sqrt{g}\boldsymbol{B}\cdot\boldsymbol{\nabla}(\xi^s)^2, \tag{10}$$

where the effective current density is defined as $\boldsymbol{K} \equiv \boldsymbol{\nabla}\times(\sigma\boldsymbol{B})$, while that for the NI model is given by

$$\delta W_{\rm J}(s) = -\frac{1}{2}\int_0^{\frac{2\pi}{L_s}} {\rm d}\phi \int_0^{2\pi} {\rm d}\theta \frac{\boldsymbol{j}_p\cdot\boldsymbol{B}}{B^2}\left[\frac{\sqrt{g}B^2}{|\boldsymbol{\nabla}s|^2}\left(\frac{\boldsymbol{j}_p\cdot\boldsymbol{B}}{B^2}\right) + \psi'(s)\Phi''(s) - \Phi'(s)\psi''(s)\right](\xi^s)^2$$
$$-\frac{1}{2}\int_0^{\frac{2\pi}{L_s}} {\rm d}\phi \int_0^{2\pi} {\rm d}\theta \frac{\boldsymbol{j}_p\cdot\boldsymbol{B}}{B^2} h_s\sqrt{g}\boldsymbol{B}\cdot\boldsymbol{\nabla}(\xi^s)^2, \tag{11}$$

where the $(\boldsymbol{j}_p\cdot\boldsymbol{B})\boldsymbol{B}/B^2$ is the projection of the current density vector parallel to the equilibrium magnetic field lines contributed by just the thermal species of the plasma [17]. The kink driving term in the KO model includes the full effective parallel current density $\boldsymbol{K}\cdot\boldsymbol{B}/B^2$. In the NI model, only the current density attributed to the thermal species in the plasma contributes to the instability dynamics [5]. This constitutes the sole difference between the two models adopted with respect to the perturbed energy associated with kink modes. The term $\psi'(s)\Phi''(s) - \Phi'(s)\psi''(s)$ is related to the global magnetic shear and $h_s \equiv [I(s)g_{s\theta} + J(s)g_{s\phi}]/(\sqrt{g}\sigma|\boldsymbol{\nabla}s|^2)$ constitutes the integrated residual local magnetic shear.

5. Applications to a 10-period Heliotron

The effects of large pressure anisotropies induced by energetic particle species on the equilibrium and fluid stability properties are investigated for a 10-field period Heliotron that has served as a useful model of the LHD [11]. In addition to the thermal pressure $p(s)$ and the hot particle scale factor $p_{\rm h}(s)$ profiles, we choose the effective toroidal current $2\pi J$ to vanish on each flux surface. We adjust the input parameters $p(0)$, $p_{\rm H}$ (where $p_{\rm H}$ corresponds to the amplitude factor of $p_{\rm h}(s)$) and $T_\perp/T_\parallel$ to achieve conditions for which $\langle\beta\rangle \equiv \int {\rm d}^3x\mu_0(p_\parallel + p_\perp)/\int {\rm d}^3x B^2 \simeq 4\%$ $\langle\beta_{\rm th}\rangle \equiv \int {\rm d}^3x 2\mu_0 p/\int {\rm d}^3x B^2 \simeq 2.6\%$ and $\langle\beta^{\rm h}_\perp\rangle/\langle\beta^{\rm h}_\parallel\rangle$ is approximately either 3.6 or 1/3.6.

5.1. Profile effects for on-axis hot particle pressure deposition

The evaluation and comparison of hot particle pressure profile effects for large parallel and perpendicular pressure anisotropies reveal that $n = 3$ global mode family structures are more unstable than the $n = 1$, 2 and 4 mode families. The hot particle pressure profiles are given

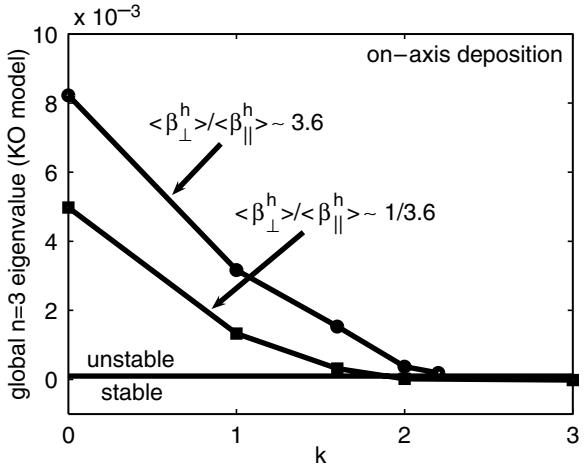

Figure 2. The converged global $n = 3$ eigenvalue according to the KO model for large parallel anisotropy $\langle\beta_\perp^{\rm h}\rangle/\langle\beta_\parallel^{\rm h}\rangle \simeq 1/3.6$ (squares) and for large perpendicular anisotropy $\langle\beta_\perp^{\rm h}\rangle/\langle\beta_\parallel^{\rm h}\rangle \simeq 3.6$ (dots) as a function of the hot particle pressure peakedness factor k for central fast particle deposition.

by $p_{\rm h}(s) \propto (1-s)^k$ for integer values of k and $p_{\rm h}(s) \propto (1-\alpha)(1-s)^{\ell+1} + \alpha(1-s)^\ell$ for non-integer values of k where ℓ is equal to the nearest lower integer corresponding to k and α is a parameter that varies from 0 to 1. The thermal pressure profile is chosen as $p(s) = p(0)(1-s)(1-s^4)$ which approximates the experimental conditions [18]. The critical magnetic field for on-axis deposition corresponds to $B_{\rm C} = 2.7\,{\rm T}$. The converged unstable global $n = 3$ eigenvalues as a function of k which governs the peakedness of the hot particle pressure profiles for $\langle\beta_\perp^{\rm h}\rangle/\langle\beta_\parallel^{\rm h}\rangle \simeq 3.6$ and $1/3.6$ are displayed in figure 2 according to the KO model. This shows that marginal stability is achieved with slightly broader profiles when $p_\parallel > p_\perp$. The marginally stable fast particle pressure profiles from the KO model for the cases $\langle\beta_\perp^{\rm h}\rangle/\langle\beta_\parallel^{\rm h}\rangle \simeq 3.6$ (marginally stable for $k \sim 2.2$) and $1/3.6$ (marginally stable for $k \sim 1.6$) are shown in figure 3. The NI model predicts that at $\langle\beta\rangle \simeq 4\%$ and $\langle\beta^{\rm h}\rangle/\langle\beta\rangle \simeq 1/3$, the plasma is stable to global and local MHD modes for both anisotropy cases. The KO model can also predict stability; however, the energetic particle profiles must be sufficiently more peaked than the thermal pressure profiles to achieve this condition.

5.2. Applications to off-axis energetic particle pressure deposition

We investigate the effects of off-axis hot particle pressure deposition on the HF side and the LF side for cases with large parallel $\langle\beta_\perp^{\rm h}\rangle/\langle\beta_\parallel^{\rm h}\rangle \simeq 1/3.6$ and with large perpendicular $\langle\beta_\perp^{\rm h}\rangle/\langle\beta_\parallel^{\rm h}\rangle \simeq 3.6$ pressure anisotropy on the equilibrium, local and global stability properties of a 10-field period Heliotron configuration in this subsection. HF fast particle deposition is realized with the choice $B_{\rm C} = 3.1\,{\rm T}$, while LF deposition occurs when $B_{\rm C} = 2.3\,{\rm T}$. We also compare the results with a reference case of central hot particle deposition for which $B_{\rm C} = 2.7\,{\rm T}$, $\langle\beta_\perp^{\rm h}\rangle/\langle\beta_\parallel^{\rm h}\rangle \simeq 1/3.6$ and the parameter k that controls the peakedness of the hot particle pressure profile is chosen as unity. The thermal pressure profile chosen has been described in the previous subsection and the hot particle pressure scale factor is $p_{\rm h}(s) = p_{\rm H}s(1-s)$.

We specifically consider twelve different cases in this subsection based on two physics models (KO and NI), two pressure anisotropies ($p_\parallel > p_\perp$ and $p_\perp > p_\parallel$) and three hot

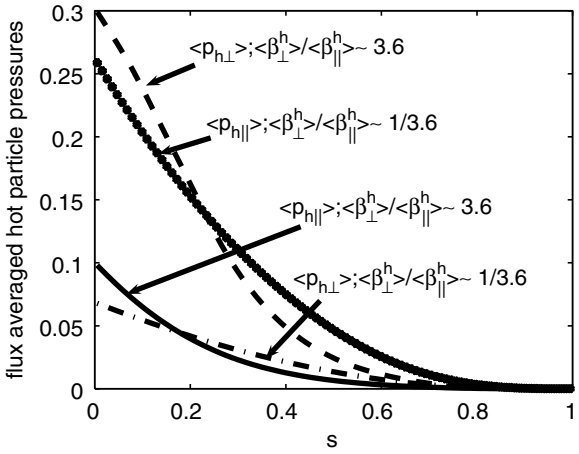

Figure 3. The flux surface averaged perpendicular $p_{\mathrm{h}\perp}$ and parallel $p_{\mathrm{h}\parallel}$ hot particle pressure profiles that are marginally stable to global $n = 3$ modes for large parallel anisotropy $\langle\beta^{\mathrm{h}}_{\perp}\rangle/\langle\beta^{\mathrm{h}}_{\parallel}\rangle \simeq 1/3.6$ ($\langle p_{\mathrm{h}\parallel}\rangle$:dotted curve ;$\langle p_{\mathrm{h}\perp}\rangle$:dotted–dashed curve) and for large perpendicular anisotropy $\langle\beta^{\mathrm{h}}_{\perp}\rangle/\langle\beta^{\mathrm{h}}_{\parallel}\rangle \simeq 3.6$ ($\langle p_{\mathrm{h}\parallel}\rangle$:solid curve ;$\langle p_{\mathrm{h}\perp}\rangle$:dashed curve) with central fast particle deposition.

particle deposition zones (LF, on-axis, HF). We shall discover that the equilibrium properties (i.e. rotational transform, magnetic well profiles) of off-axis HF side deposition and LF side deposition with $p_{\parallel} > p_{\perp}$ are very similar to one with another. The ensuing fluid stability properties within each physics model are correspondingly very similar. The cases associated with $p_{\perp} > p_{\parallel}$ LF side deposition and on-axis deposition, on the other hand, display equilibrium properties that differ noticeably; therefore, their stability properties are significantly modified.

The rotational transform profiles for the cases investigated are shown in figure 4(*a*). For on-axis energetic particle deposition with $p_{\parallel} > p_{\perp}$, the magnetic shear is negative in the inner half and positive in the outer half of the plasma volume. For LF side deposition and large perpendicular anisotropy ($\langle\beta^{\mathrm{h}}_{\perp}\rangle/\langle\beta^{\mathrm{h}}_{\parallel}\rangle \simeq 3.6$), the magnetic shear is positive in the inner and outer $1/3$ fraction of the plasma volume and weakly negative in between. For the other off-axis hot particle deposition cases, the rotational transform profiles are very similar to each other with positive shear in the inner quarter and outer third of the plasma volume with almost vanishing shear in between. The differential volume profiles in figure 4(*b*) demonstrate that the system with central fast particle deposition has a magnetic well (a negative derivative of the differential volume with respect to s) in the inner 60% and a magnetic hill in the outer 40% of the plasma volume. For LF side and large perpendicular anisotropy ($\langle\beta^{\mathrm{h}}_{\perp}\rangle/\langle\beta^{\mathrm{h}}_{\parallel}\rangle \simeq 3.6$), the differential volume profile displays a strong and extended magnetic hill core region, a strong edge magnetic hill region and a relatively deep magnetic well connecting region. For the remaining off-axis deposition cases, the differential volume profiles are very similar to each other. The shapes of these profiles follow that of the $p_{\perp} > p_{\parallel}$ LF side hot particle deposition case, but with weaker plasma core and periphery hill regions and weaker magnetic well region in between. A rationale for the similarity of the equilibrium and resulting stability properties of HF off-axis and $p_{\parallel} > p_{\perp}$ LF side deposition from a particle perspective is deferred to the next section. The mod-B contours and the perpendicular hot particle pressures for HF and LF deposition on three cross-sections of the Heliotron system under investigation are displayed in figure 5 for $\langle\beta^{\mathrm{h}}_{\perp}\rangle/\langle\beta^{\mathrm{h}}_{\parallel}\rangle \simeq 3.6$. For HF side deposition, the distribution of $p_{h\perp}$ shows that the hot particles can cover most of the flux surface they reside on, whilst this is not the case for LF side deposition.

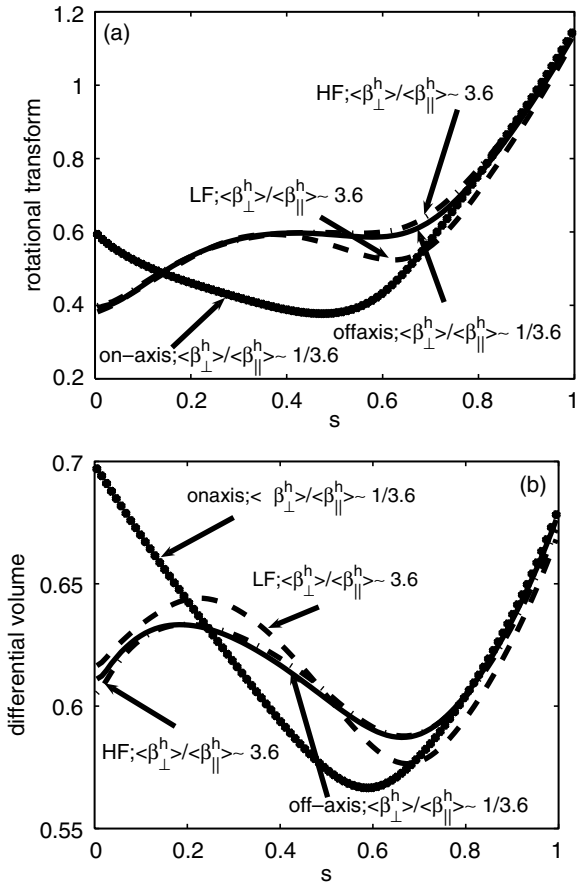

Figure 4. The rotational transform (*a*) and the differential volume (*b*) profiles in a 10-period Heliotron with $\langle\beta_{\rm th}\rangle \simeq 2.63\%$ and $\langle\beta\rangle \simeq 4\%$ for on-axis (large dotted curve) and off-axis (solid curve) hot particle deposition with large parallel anisotropy ($\langle\beta_\perp^{\rm h}/\langle\beta_\parallel^{\rm h}\rangle \sim 1/3.6$) and for HF (dotted–dashed curve) and LF (dashed curve) side hot particle deposition with large perpendicular anisotropy ($\langle\beta_\perp^{\rm h}/\langle\beta_\parallel^{\rm h}\rangle \sim 3.6$).

Stability studies with respect to global $n = 2$ mode family structures and the Mercier criterion with the application of the KO and NI models have been carried out for the off-axis hot particle deposition cases. Although $n = 3$ modes are somewhat more unstable than the $n = 2$ modes presented here, the conclusions that can be drawn from this investigation remain insensitive to the structure explored under conditions that are far from marginal stability. The perturbed potential energy $\delta W_{\rm P}$ profiles (for which negative values indicate instability) are shown for the KO model with large parallel anisotropy $\langle\beta_\perp^{\rm h}\rangle/\langle\beta_\parallel^{\rm h}\rangle \simeq 1/3.6$ in figure 6(*a*), with large perpendicular anisotropy $\langle\beta_\perp^{\rm h}\rangle/\langle\beta_\parallel^{\rm h}\rangle \simeq 3.6$ in figure 6(*b*) and for the NI model in figure 7. In both models, the broadest profile (and consequently the most unstable) corresponds to that of large perpendicular anisotropy and LF fast particle deposition. The KO model case with $\langle\beta_\perp^{\rm h}\rangle/\langle\beta_\parallel^{\rm h}\rangle \simeq 3.6$ and HF deposition shows a correspondingly much more localized unstable domain. The large parallel anisotropy cases ($\langle\beta_\perp^{\rm h}\rangle/\langle\beta_\parallel^{\rm h}\rangle \simeq 1/3.6$) display a δW_P profile that lie in between the two $\langle\beta_\perp^{\rm h}\rangle/\langle\beta_\parallel^{\rm h}\rangle \simeq 3.6$ cases but with smaller maximum absolute amplitude. The on-axis hot particle deposition case has an oscillatory $\delta W_{\rm P}$ profile with small maximum

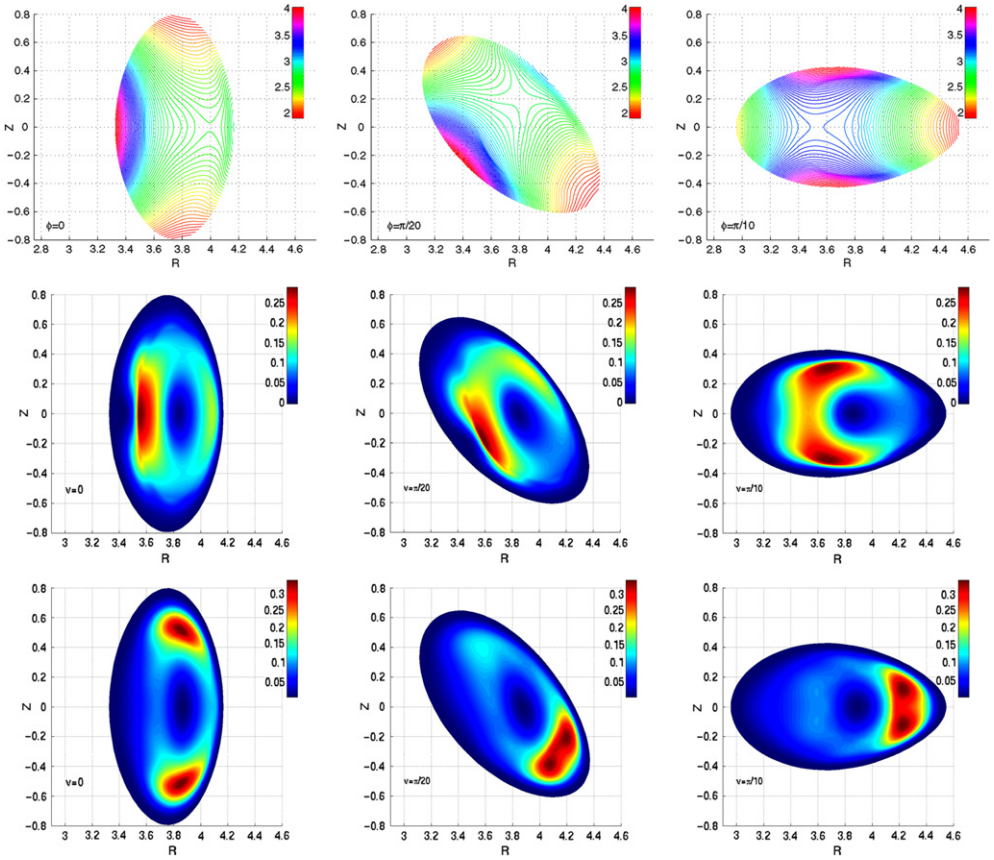

Figure 5. The contours of the modulus of the magnetic field strength B (top row) and the distributions of the perpendicular energetic particle pressure $p_{\mathrm{h}\perp}$ for HF (middle row) and LF (bottom row) side hot particle deposition at three cross sections ($v = 0$, left), ($v = \pi/20$, middle) and ($v = \pi/10$, right) that span half of a field period in a Heliotron configuration at $\langle\beta_{\mathrm{th}}\rangle \simeq 2.63\%$, $\langle\beta\rangle \simeq 4\%$ and $\langle\beta_{\perp}^{\mathrm{h}}\rangle/\langle\beta_{\parallel}^{\mathrm{h}}\rangle \simeq 3.6$.

(This figure is in colour only in the electronic version)

absolute amplitude. The global instability structures are localized at about 2/3 of the plasma volume in a region with finite total pressure gradient, weak magnetic shear and transition from magnetic well to magnetic hill. For the NI model, the on-axis deposition case is stable (only a small negative spike is observed at $s \sim 2/3$). The off-axis $\langle\beta_{\perp}^{\mathrm{h}}\rangle/\langle\beta_{\parallel}^{\mathrm{h}}\rangle \simeq 1/3.6$ and the HF $\langle\beta_{\perp}^{\mathrm{h}}\rangle/\langle\beta_{\parallel}^{\mathrm{h}}\rangle \simeq 3.6$ cases in the NI model have almost identical δW_{P} profiles that are very narrow and concentrate near the plasma core. The LF $\langle\beta_{\perp}^{\mathrm{h}}\rangle/\langle\beta_{\parallel}^{\mathrm{h}}\rangle \simeq 3.6$ case has a broader profile than the other cases considered, a comparable maximum absolute amplitude for δW_{P} and is thus more unstable.

The Mercier criterion is consistent with the global $n = 2$ mode family stability properties previously described both for the KO and NI models. The Mercier criterion profiles for the cases investigated are presented in figure 8(*a*) for the KO model and in figure 8(*b*) for the NI model. The reference on-axis large parallel anisotropy ($\langle\beta_{\perp}^{\mathrm{h}}\rangle/\langle\beta_{\parallel}^{\mathrm{h}}\rangle \simeq 1/3.6$) case is stable within the NI model and shows a small region of instability in the KO model around $s \sim 3/4$. The off-axis $\langle\beta_{\perp}^{\mathrm{h}}\rangle/\langle\beta_{\parallel}^{\mathrm{h}}\rangle \simeq 1/3.6$ HF and LF cases are almost the same displaying moderately

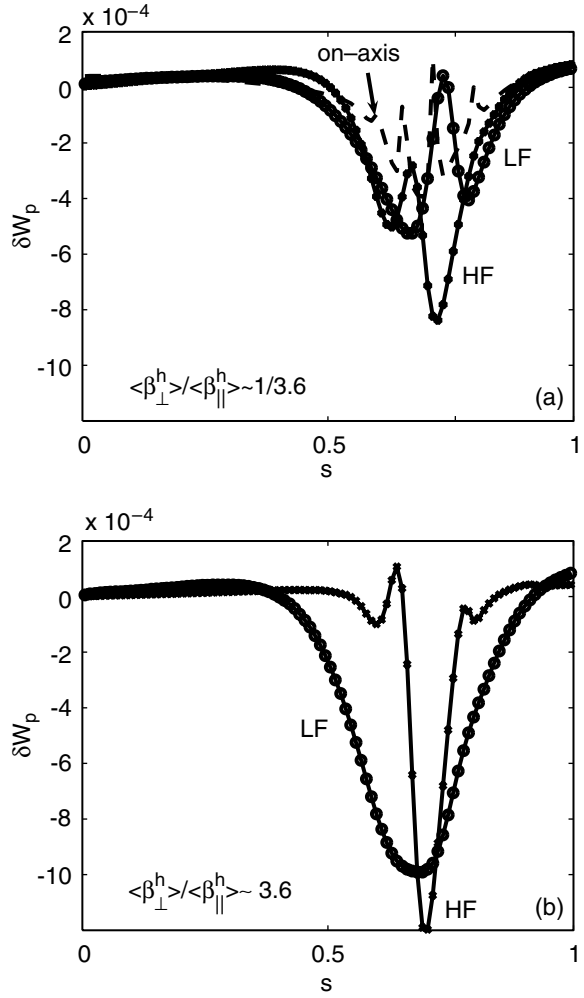

Figure 6. The perturbed potential energy δW_{P} profiles according to the KO model at $\langle\beta_{\mathrm{th}}\rangle \simeq 2.63\%$ and $\langle\beta\rangle \simeq 4\%$ for on-axis (dashed curves), LF (large dotted curves) and HF (small dotted curves) hot particle deposition cases with (*a*) large parallel ($\langle\beta_{\perp}^{\mathrm{h}}/\langle\beta_{\parallel}^{\mathrm{h}}\rangle \sim 1/3.6$) and (*b*) perpendicular pressure anisotropy ($\langle\beta_{\perp}^{\mathrm{h}}/\langle\beta_{\parallel}^{\mathrm{h}}\rangle \sim 3.6$).

weak instability in the inner 90% of the plasma volume according to the KO model (for the sake of clarity only one of the two cases is plotted in figure 8(*b*)). The HF $\langle\beta_{\perp}^{\mathrm{h}}\rangle/\langle\beta_{\parallel}^{\mathrm{h}}\rangle \simeq 3.6$ ($p_{\perp} > p_{\parallel}$) case is somewhat more unstable in this model except for a small region near mid-volume. The LF $\langle\beta_{\perp}^{\mathrm{h}}\rangle/\langle\beta_{\parallel}^{\mathrm{h}}\rangle \simeq 3.6$ case is different. It is stable in the inner third of the plasma volume, but more unstable than the other off-axis hot particle deposition cases considered in the outer 2/3 fraction of the plasma volume. The positive hot particle pressure gradients in the core reduce the instability drive in this region for the KO model (see figure 1). In the NI model, the hot particles do not interact and the thermal pressure gradient is not opposed by that of the fast particles in the central region of the plasma which implies that all of the off-axis hot particle deposition cases investigated are Mercier unstable mainly in the plasma core according to this model. The instability is driven by the thermal pressure gradients in the central region of the plasma and is more strongly unstable than the KO model prediction because of the partial

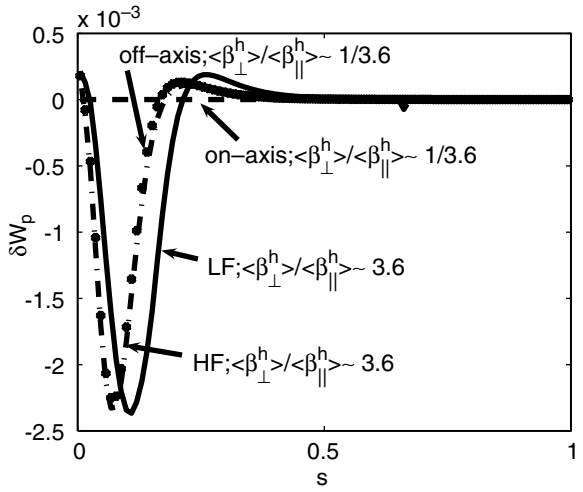

Figure 7. The perturbed potential energy δW_{P} profiles according to the NI model at $\langle\beta_{\mathrm{th}}\rangle \simeq 2.63\%$ and $\langle\beta\rangle \simeq 4\%$ for off-axis (dotted curves) and on-axis (dashed curves) cases with large parallel pressure anisotropy ($\langle\beta_{\perp}^{\mathrm{h}}/\langle\beta_{\parallel}^{\mathrm{h}}\rangle \sim 1/3.6$) and for HF (dotted–dashed curves) and LF (solid curves) side cases with large perpendicular pressure anisotropy ($\langle\beta_{\perp}^{\mathrm{h}}/\langle\beta_{\parallel}^{\mathrm{h}}\rangle \sim 3.6$).

cancellation in the core of the thermal pressure gradients by the hot particle pressure gradients in the KO theory (in conjunction with the central magnetic hill that appears with off-axis hot particle deposition).

The global unstable eigenvalues with respect to global $n = 2$ modes according to the KO and NI models versus the value of B_{C} that governs the fast particle deposition layer position are shown in figure 9. The eigenvalues for the reference case of central deposition ($B_{\mathrm{C}} = 2.7$ T) are considerably smaller thus more stable than those for off-axis energetic particle deposition (at $B_{\mathrm{C}} = 2.3$ T and $B_{\mathrm{C}} = 3.1$ T). For the cases with off-axis deposition and ($\langle\beta_{\perp}^{\mathrm{h}}\rangle/\langle\beta_{\parallel}^{\mathrm{h}}\rangle \simeq 1/3.6$), the eigenvalues for the KO and NI models do not change significantly between the HF and LF cases. The NI model for these cases in which the mode is localized near the plasma centre is more unstable than the KO model where the mode is localized closer to the plasma periphery. For the HF $\langle\beta_{\perp}^{\mathrm{h}}\rangle/\langle\beta_{\parallel}^{\mathrm{h}}\rangle \simeq 3.6$ case, the global eigenvalue almost matches the HF $p_{\parallel} > p_{\perp}$ case at $B_{\mathrm{C}} = 3.1$ T according to the KO model, but for the NI model it is slightly more unstable than its $p_{\parallel} > p_{\perp}$ counterpart. For LF deposition with $\langle\beta_{\perp}^{\mathrm{h}}\rangle/\langle\beta_{\parallel}^{\mathrm{h}}\rangle \simeq 3.6$, the KO model predicts more unstable conditions than the NI model and the global eigenvalues are considerably more unstable compared with the other off-axis deposition cases examined. One important cause of the destabilization is illustrated in figure 10 which shows that for LF hot particle deposition, the extent of the destabilizing perpendicular hot particle pressure gradient is larger than the corresponding gradient for HF deposition which is sharper but more localized.

6. Conclusion and discussion

The fluid MHD equilibrium and stability properties of anisotropic pressure plasmas in 3D stellarators have been investigated with the application of the Kruskal–Oberman energy principle in which the energetic particle species that generate the anisotropy fully interact with the dynamics of the instability (the KO model) and with the application of the

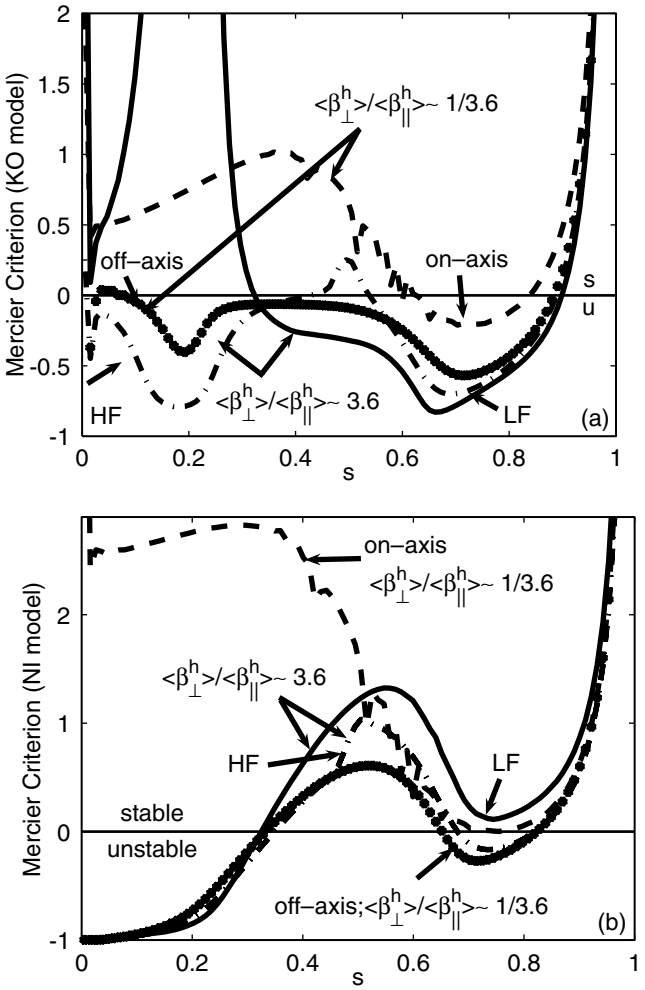

Figure 8. The Mercier criterion according to (*a*) the KO model and (*b*) the NI model in a 10-period Heliotron with $\langle\beta_{\rm th}\rangle \simeq 2.63\%$ and $\langle\beta\rangle \simeq 4\%$ for off-axis (dotted curves) and on-axis (dashed curves) cases with large parallel pressure anisotropy ($\langle\beta^{\rm h}_{\perp}/\langle\beta^{\rm h}_{\parallel}\rangle \sim 1/3.6$) and for HF (dotted–dashed curves) and LF (solid curves) side cases with large perpendicular pressure anisotropy ($\langle\beta^{\rm h}_{\perp}/\langle\beta^{\rm h}_{\parallel}\rangle \sim 3.6$).

Johnson–Kulsrud–Weimer energy principle in which the fast particles constitute a rigid non-interacting fluid (the NI model). Comparative studies of on-axis versus off-axis, of HF versus LF hot particle deposition and of large parallel versus large perpendicular pressure anisotropy have been explored.

Central hot particle deposition in a 10-field period Heliotron at $\langle\beta\rangle \simeq 4\%$ and $\langle\beta^{\rm h}\rangle/\langle\beta\rangle \simeq 1/3$ is stable to local and global fluid MHD modes according to the NI model and stability is also predicted with the KO model provided; however, the hot particle pressure profiles are sufficiently peaked. Therefore, we cannot categorically conclude at this point that the NI model constitutes a more appropriate description of the experimental results observed on the LHD compared with the KO model (which recovers the incompressible ideal MHD model in the limit $p_{\perp} = p_{\parallel}$) given the uncertainties in the energetic hot particle species pressure

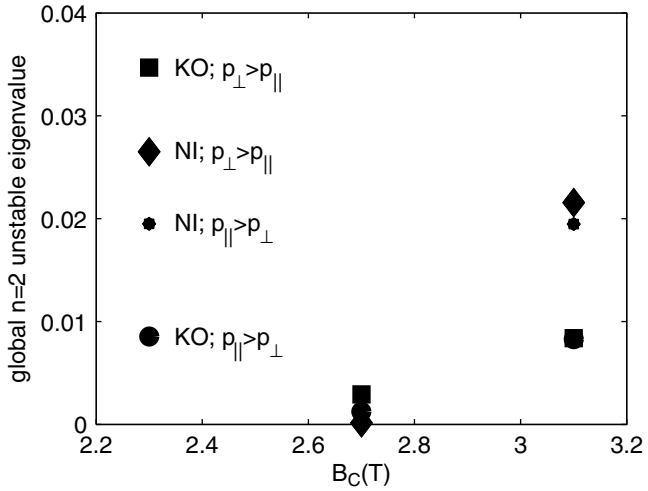

Figure 9. The global $n = 2$ eigenvalues for $\langle\beta_\perp^{\rm h}\rangle/\langle\beta_\parallel^{\rm h}\rangle \simeq 3.6$ according to the KO model (squares), according to the NI model (diamonds), for $\langle\beta_\perp^{\rm h}\rangle/\langle\beta_\parallel^{\rm h}\rangle \simeq 1/3.6$ according to the KO model (large circles) and according to the NI model (small circles) for LF ($B_{\rm C} = 2.3$ T), for on-axis ($B_{\rm C} = 2.7$ T) and for HF ($B_{\rm C} = 3.1$ T) hot particle deposition.

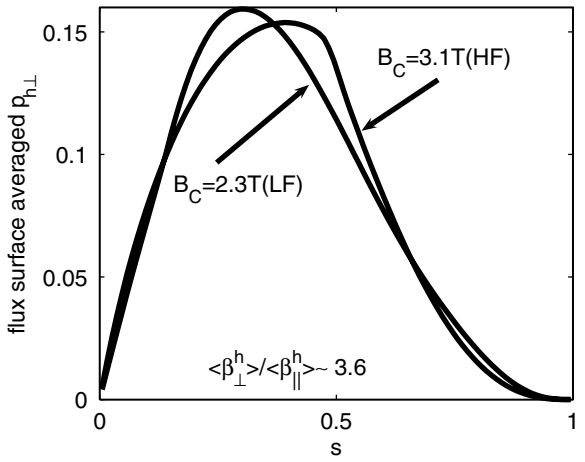

Figure 10. The flux surface averaged $p_{\rm h\perp}$ profiles for HF ($B_{\rm C} = 3.1$ T) and LF ($B_{\rm C} = 2.3$ T) hot particle deposition with $\langle\beta_\perp^{\rm h}\rangle/\langle\beta_\parallel^{\rm h}\rangle \simeq 3.6$. These profiles are near the marginal point with respect to global $n = 3$ modes according to the KO model.

profiles that have been assumed in the experimental discharges. For the KO model, we have found that global $n = 3$ mode family structures yield somewhat more severe stability limits than the $n = 1$, 2 and 4 mode families. Furthermore, under these conditions we find that the marginally stable profiles with respect to global modes are slightly broader for $p_\parallel > p_\perp$ than when $p_\perp > p_\parallel$.

Off-axis energetic particle pressure deposition destabilizes both local and global MHD modes compared with on-axis deposition where the larger core magnetic well can sustain larger near-axis pressure gradients. A core magnetic hill is produced when large hot particle pressures are concentrated around the mid-volume of the plasma. Off-axis fast particle deposition for

$p_\parallel > p_\perp$ as well as HF side deposition with $p_\perp > p_\parallel$ yield very similar rotational transform and magnetic well profiles. As a result, the global unstable eigenvalues are very similar in magnitude for these cases in a 10-field period Heliotron with $\langle\beta\rangle \simeq 4\%$ and $\langle\beta_{\rm th}\rangle \simeq 2.6\%$. These eigenvalues are significantly more unstable than those with on-axis deposition having equivalent total, thermal and hot particle $\langle\beta\rangle$ components. In the core of the plasma for off-axis fast particle deposition, the energetic particle pressure gradients partially cancel the thermal pressure gradients. This leads in the KO model to a reduced instability drive. In the NI model where the hot particles do not interact, this cancellation is missing and the remaining thermal pressure gradients fully drive global and local modes which concentrate in the centre of the plasma. The combined fast particle and thermal pressure gradients drive global and local MHD modes closer to the plasma periphery when the KO model is applied. The NI model usually yields more unstable conditions than the KO model because of the partial cancellation of the thermal pressure gradients by the energetic particles in the plasma core. LF side hot particle deposition with $p_\perp > p_\parallel$ alters the rotational transform and the magnetic well more significantly than HF deposition or off-axis deposition with $p_\parallel > p_\perp$. In cases with large perpendicular anisotropy deposited on the HF side, the energetic particles are barely trapped and sample a very large fraction of the field lines they reside on. Therefore, they almost behave like circulating particles and this can in large part explain the similarity of the equilibrium and stability properties of HF side hot particle deposition with $p_\perp > p_\parallel$ compared with off-axis (HF or LF side) deposition with $p_\parallel > p_\perp$. In cases with large perpendicular anisotropy deposited on the LF side, the energetic particles are deeply trapped and only sample a limited extent of the field lines they reside on. Thus, the equilibrium and stability behaviour is different from HF side deposition with $p_\perp > p_\parallel$ or when $p_\parallel > p_\perp$. The global eigenvalues are significantly more unstable for the $p_\perp > p_\parallel$ LF side deposition case. The more extended gradients of the hot perpendicular pressure that encompasses a larger fraction of the weak magnetic shear region broadens the mode structure in the KO model causing it to become more unstable compared with $p_\parallel > p_\perp$ cases or HF side $p_\perp > p_\parallel$ deposition cases. The more extended core magnetic hill in the LF side $p_\perp > p_\parallel$ deposition case broadens the mode structure in the NI model making it correspondingly more unstable than the other cases examined with the rigid hot particle treatment. The KO model under these circumstances remains more unstable than the NI model.

Substantial off-axis fast particle deposition should provide a more definitive answer to the validity of the KO or NI models to describe the experimental conditions in Heliotron systems like LHD. If the dominant low order mode structure detected concentrates near the plasma periphery, the KO model (and therefore in some sense the ideal MHD model that has been regularly applied to the discharges) would be more appropriate than the NI model. The converse holds true if the dominant low order mode structure is localized towards the plasma core.

Acknowledgments

This research was partially sponsored by the Fonds National Suisse de la Recherche Scientifique and Euratom. We thank Dr S P Hirshman for use of the VMEC code.

References

[1] Watanabe K Y *et al* and LHD experimental group 2005 *Nucl. Fusion* **45** 1247
[2] Yamaguchi T *et al* and LHD experimental group 2005 *Nucl. Fusion* **45** L33

[3] Kruskal M D and Oberman C R 1958 *Phys. Fluids* **1** 275
[4] Spies G O and Nelson D B 1974 *Phys. Fluids* **17** 1865
[5] Johnson J L, Kulsrud R M and Weimer K 1969 *Plasma Phys.* **11** 463
[6] Nelson D B and Hedrick C L 1979 *Nucl. Fusion* **19** 285
[7] Dendy R O, Hastie R J, McClements K G and Martin T J 1995 *Phys. Plasmas* **2** 1623
[8] McClements K G, Dendy R O, Hastie R J and Martin T J 1996 *Phys. Plasmas* **3** 2994
[9] Graves J P, Hopkraft K I, Dendy R O, Hastie R J, McClements K G and Mantsinen M 2000 *Phys. Rev. Lett.* **84** 1204
[10] Cooper W A *et al* 2006 *Nucl. Fusion* **46** 683
[11] Nakamura Y *et al* 1996 *J. Comput. Phys.* **128** 43
[12] Hirshman S P and Whitson J C 1983 *Phys. Fluids* **26** 3553
[13] Cooper W A *et al* 2006 *Fusion Sci. Technol.* **50** 245
[14] Nührenberg C (née Schwab) 1992 *Proc. Varenna–Lausanne Int. Workshop on Theory of Fusion Plasmas (Varenna, Italy, 24–28 August 1992)* (Bologna: Editrice Compositori) p 383
Cooper W A *et al* 2003 *J. Plasma Fusion Res. Ser.* **6** 152
[15] Boozer A H 1980 *Phys. Fluids* **23** 904
[16] Grad H 1966 *Phys. Fluids* **9** 498
[17] Cooper W A 1992 *Plasma Phys. Control. Fusion* **34** 1011
[18] Watanabe K Y *et al* and LHD experimental group 2004 *Fusion Sci. Technol.* **46** 24